Accepted Manuscript

Computational analysis of magnetohydrodynamic natural convection in a square cavity with a thin fin

S.M. Aminossadati, B. Ghasemi, A. Kargar

PII: S0997-7546(14)00037-5
DOI: http://dx.doi.org/10.1016/j.euromechflu.2014.03.002
Reference: EJMFLU 2752

To appear in: *European Journal of Mechanics B/Fluids*

Received date: 18 May 2012
Revised date: 5 March 2014
Accepted date: 10 March 2014

Please cite this article as: S.M. Aminossadati, B. Ghasemi, A. Kargar, Computational analysis of magnetohydrodynamic natural convection in a square cavity with a thin fin, *European Journal of Mechanics B/Fluids* (2014), http://dx.doi.org/10.1016/j.euromechflu.2014.03.002

Highlights

- Magnetohydrodynamic laminar natural convection in a square cavity with a fin is examined
- Three numerical approaches of ANFIS, ANN and CFD are used in the investigation
- ANFIS and ANN accurately predict the cavity's thermal performance in less time
- Magnetic field affects natural convection especially at higher Rayleigh numbers
- Fin's length and position significantly affect the heat transfer rate of the cavity

Graphical Abstract (for review)

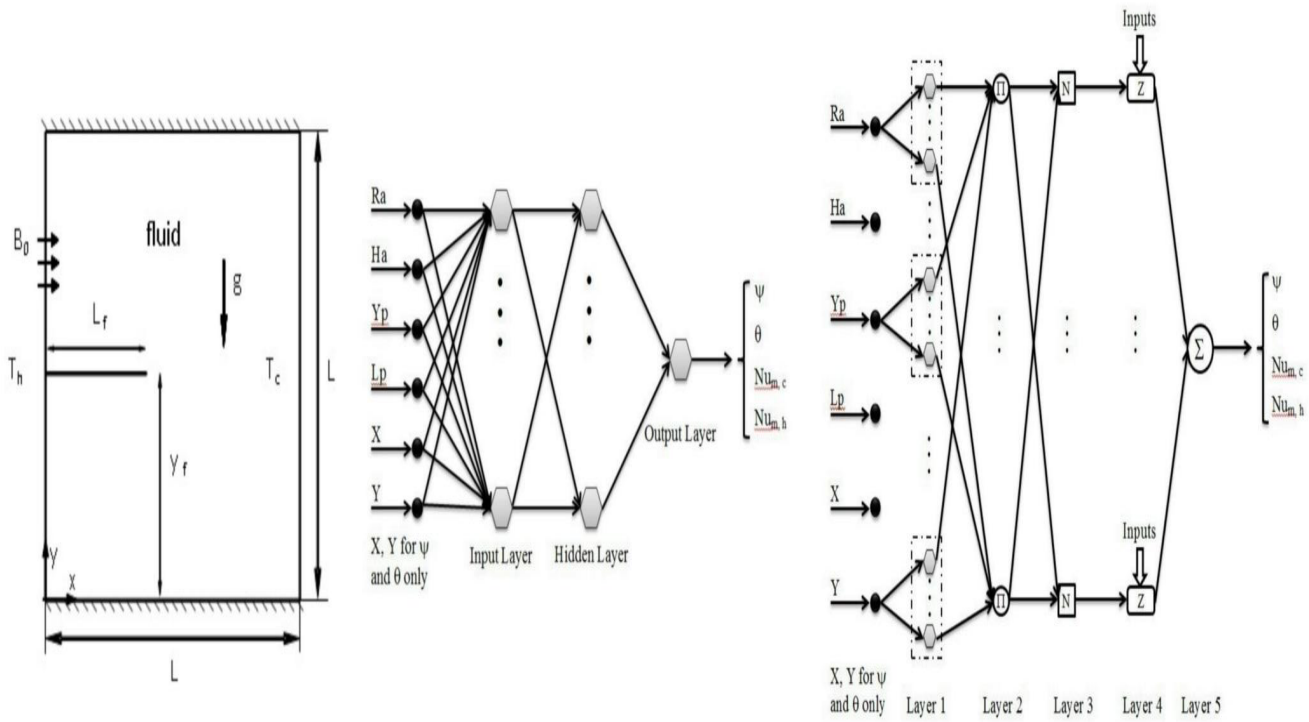

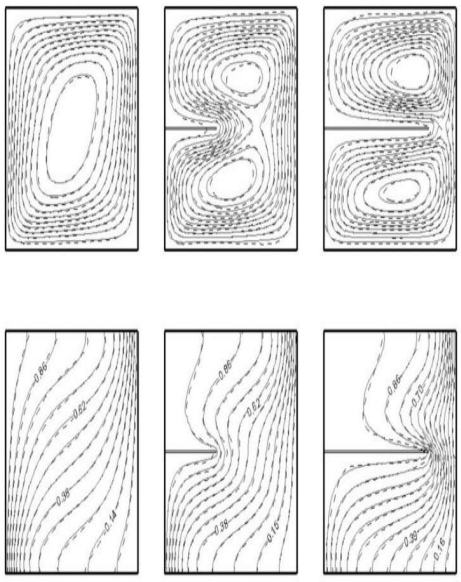

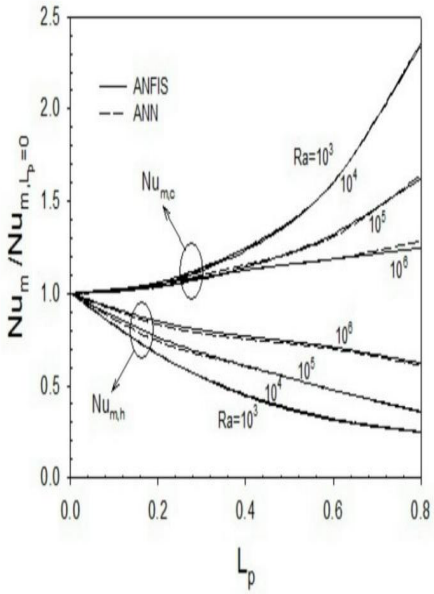

Computational Analysis of Magnetohydrodynamic Natural Convection in a Square Cavity with a thin fin

S.M. Aminossadati
Senior Lecturer, School of Mechanical and Mining Engineering, The University of Queensland, QLD 4072, Australia
E-Mail: uqsamino@uq.edu.au
Tel:+61-7-33653676
Fax:+61-7-33653888

B. Ghasemi
Associate Professor, Engineering Faculty, Shahrekord University, Shahrekord, P.O.Box 115, Iran
E-Mail: behzadgh@yahoo.com
Tel/Fax: +98-381-4424438

A. Kargar
Assistant Professor, Engineering Faculty, Shahrekord University, Shahrekord, P.O.Box 115, Iran
E-Mail: kargar@ieee.org
Tel/Fax: +98-381-4424438

Abstract

A numerical study of laminar natural convection in a square cavity with a thin fin that is under the influence of a uniform magnetic field is presented. The side walls of the cavity are kept at different temperatures and the horizontal walls are thermally insulated. An Adaptive Network-based Fuzzy Inference System (ANFIS) approach and an Artificial Neural Network (ANN) approach are developed, trained and validated using the results of Computational Fluid Dynamics (CFD) analysis. The effects of pertinent parameters on fluid flow and heat transfer characteristics are studied. Among these parameters are the Rayleigh number ($10^3 \le \mathrm{Ra} \le 10^6$), the Hartmann number ($0 \le \mathrm{Ha} \le 100$), the position of the thin fin ($0.1 \le Y_p \le 0.9$) and the length of the thin fin ($0 \le L_p \le 0.8$). The results show that ANFIS and ANN can successfully predict the fluid flow and heat transfer behaviour within the cavity in less time without compromising accuracy. In most cases, ANFIS can predict the results more accurately than ANN.

Keywords: Natural convection; Square cavity; Magnetohydrodynamic; ANFIS; ANN; CFD

Nomenclature

B_0	magnetic field strength
C_p	specific heat, $J\,kg^{-1}\,K^{-1}$
g	gravitational acceleration, $m\,s^{-2}$
Ha	Hartmann number ($B_0 L\sqrt{\sigma/\rho\nu}$)
k	thermal conductivity, $W\,m^{-1}K^{-1}$
L	length of the cavity, m
L_f	length of the fin, m
L_p	dimensionless length of the fin (L_f/L)
N	the number of data in the data set (Eq. 9)
Nu	local Nusselt number
p	fluid pressure, Pa
$\bar{p}$	modified pressure ($p+\rho_c gy$)
P	dimensionless pressure ($\bar{p}L^2/\rho\alpha^2$)
Pr	Prandtl number (ν/α)
Ra	Rayleigh number $(g\beta L^3(T_h - T_c)/\nu\alpha)$
S_p	dimensionless vertical distance of the fin from the top wall ($1 - Y_P$)
T	temperature, K
u, v	velocity components in x and y directions, $m\,s^{-1}$
U, V	dimensionless velocity components ($uL/\alpha, vL/\alpha$)
x, y	Cartesian coordinates, m
y_f	vertical distance of the fin from the bottom wall, m
X, Y	dimensionless coordinates ($x/L, y/L$)
Y_p	dimensionless vertical distance of the fin from the bottom wall (y_f/L)

Greek symbols

α	thermal diffusivity, $m^2\,s^{-1}$ ($k/\rho C_p$)
β	thermal expansion coefficient, K^{-1}
μ	dynamic viscosity, $N\,s\,m^{-2}$
θ	dimensionless temperature $(T - T_c)/(T_h - T_c)$

ρ	density, kgm^{-3}
σ	electrical conductivity, $\mu S/cm$
ν	kinematic viscosity, $m^2 s^{-1}$ (μ/ρ)
ω	the calculated value of the parameter obtained from CFD
ω_m	the average of ω
ω_p	the predicted value of the parameter obtained from ANFIS or ANN
ψ	stream function

Subscripts

c	cold wall
f	fin
h	hot wall
m	average
max	maximum

1. Introduction

There is an increasing level of interest among the researchers in understanding the flow behaviour and the heat transfer mechanism of electrically conducting fluids in cavities that are located in magnetic fields [1-6]. Information related to this could be applied to many engineering problems, such as those involving the crystal growth in fluids, the metal casting, the fusion reactors and the geothermal energy extractions. The common finding of previous studies in this field is that the convective heat transfer is influenced by the magnetic field. It has also been found that the orientation and the aspect ratio of the cavity, as well as the strength and direction of the magnetic field, all affect the flow and temperature fields [7-12]. These studies have simulated the heat transfer in various geometries using Computational Fluid Dynamics (CFD), which in turn requires long computational times and large memory allocations.

Recently, numerical modelling techniques such as artificial intelligence systems have demonstrated an ability to deal with non-linear engineering problems and to reduce the cost and time of the analysis. An Artificial Neural Network (ANN) system is an information-processing paradigm that operates like a biological nervous system and simulates the neural activities in the human brain [13, 14]. ANN simulations generally draw from experimental findings, observations and records of engineering problems. However, some studies reported in the literature use the data obtained from the numerical modellings to train and test the ANN simulations and to expand the numerical results [15, 16].

Mahmoud and Ben-Nakhi [17] studied the feasibility of using ANN networks to predict the complete thermal and flow characteristics of natural convection in a portioned cavity. They trained and tested the ANN architectures using the results of CFD simulations. They demonstrated that ANN could accurately predict the natural convection parameters with a significant reduction in the analysis time and effort. Sudhakar et al. [18] also employed ANN to examine the influence of positioning of five discrete heat sources on the wall of a three-dimensional vertical duct in which the heat transfer was due to mixed convection. They used the temperature database, which was developed from CFD simulations, to train the neural network. They concluded that the trained neural network could predict the temperature of the heat sources very accurately; it was also much faster than the CFD analysis. In another study, Ozsunar et al. [19] trained and tested a neural network approach using the results of CFD simulations in order to find suitable thickness levels and materials for a chip subjected to a constant heat power. They concluded that ANN was an efficient and time-saving method compared to the CFD analysis.

ANNs have self-learning and non-linear estimation abilities, but they lack the ability to infer. This means an ANN requires massive quantities of training data, the inputting of which is an intensive and time-consuming process. The Fuzzy Logic Inference System (FIS), on the other hand, is a fast approach to solving fuzzy and uncertain problems. However, it is basically dependent on the experience of experts; it is particularly challenging to produce forecasting results when the information provided is insufficient. The Adaptive Network-Based Fuzzy Inference System (ANFIS) proved to be a robust approach, as it has the superior capabilities of ANN and FIS. It achieves more accurate modelling than the conventional time series and regression methods [20, 21].

Varol et al. [22] presented a comparison study of the results of ANN, ANFIS and CFD when analysing the natural convection characteristics in a triangular enclosure. They claimed that ANN and ANFIS were both capable of accurately predicting the flow and thermal behaviour within the enclosure, and that the results obtained from ANFIS were more accurate than ANN. In a similar study, Varol et al. [23] showed that ANFIS could significantly reduce the computation time and memory space required for the analysis of a buoyancy-induced flow field in a triangular enclosure without sacrificing the accuracy of the results.

The present study is motivated by the need to develop a fast and accurate solution for the heat transfer problem in a square cavity with a thin fin that is under the influence of a magnetic field. This study focuses on examining the effects of the length and position of the fin on the heat transfer performance of the cavity by using the ANN and ANFIS techniques. As such, a CFD simulation is carried out and the CFD results are used to train and test the ANN and ANFIS analyses. A comparison study of the accuracy and the computation time of these methods is also presented.

2. Mathematical Formulation

Figure 1 shows the schematic diagram of a two-dimensional square cavity with a thin fin that is considered in this study. The left vertical wall of the cavity is at a relatively high temperature (T_h), the right vertical wall is at a relatively low temperature (T_c), and the horizontal walls are thermally insulated. The temperature of the fin is also assumed to be T_h (fin with a high thermal conductivity). The cavity is filled with pure water ($Pr = 6.2$) and is under the influence of a magnetic field with a uniform strength (B_0). The displacement currents, induced magnetic field, dissipation and Joule heating are neglected. The density variation in the buoyancy forces is determined by using the Boussinesq approximation.

The steady-state equations that govern the conservation of mass, momentum and energy for the laminar natural convection of fluid in the presence of a magnetic field can be written in the following non-dimensional forms:

$$\frac{\partial U}{\partial X} + \frac{\partial V}{\partial Y} = 0 \tag{1}$$

$$\frac{\partial (U^2)}{\partial X} + \frac{\partial (UV)}{\partial Y} = -\frac{\partial P}{\partial X} + Pr\nabla^2 U \tag{2}$$

$$\frac{\partial (UV)}{\partial X} + \frac{\partial (V^2)}{\partial Y} = -\frac{\partial P}{\partial Y} + Pr\,\nabla^2 V + Ra\ Pr\ \theta - Ha^2\ Pr\ V \tag{3}$$

$$\frac{\partial (U\theta)}{\partial X} + \frac{\partial (V\theta)}{\partial Y} = \nabla^2 \theta \tag{4}$$

In the above equations the following non-dimensional parameters are used:

$$X = \frac{x}{L}, \qquad Y = \frac{y}{L}, \qquad U = \frac{u\,L}{\alpha}, \qquad V = \frac{v\,L}{\alpha}, \qquad P = \frac{\bar{p}\,L^2}{\rho\alpha^2}$$

$$\theta = \frac{T - T_c}{T_h - T_c}, \qquad Ra = \frac{g\beta L^3 (T_h - T_c)}{\nu\alpha}, \qquad Ha = B_0 L\sqrt{\frac{\sigma}{\rho\nu}}, \qquad Pr = \frac{\nu}{\alpha} \tag{5}$$

where the Rayleigh number (Ra) is an indication of the effects of buoyancy forces and the Hartmann number (Ha) corresponds to the effects of magnetic forces. The governing equations (1)-(4) are subject to the following boundary conditions:

For left wall and fin: $U = V = 0$ and $\theta = 1$

For right wall: $U = V = 0$ and $\theta = 0$

For horizontal walls: $U = V = 0$ and $\frac{\partial \theta}{\partial Y} = 0$ (6)

The local Nusselt number on the left hot wall and the right cold wall can be defined by:

$$Nu_h(Y) = -\left(\frac{\partial \theta}{\partial X}\right)_{X=0}, \qquad Nu_c(Y) = -\left(\frac{\partial \theta}{\partial X}\right)_{X=1} \tag{7}$$

The average Nusselt numbers are determined by integrating the local Nusselt numbers along the hot and cold walls:

$$Nu_{m,h} = \int_0^1 Nu_h(Y)\,dY, \qquad Nu_{m,c} = \int_0^1 Nu_c(Y)\,dY \tag{8}$$

3. CFD Approach and Validation

The non-dimensional governing equations (1)-(4) along with the boundary conditions (Eq. 6) are solved by the control volume formulation using Patankar's SIMPLE algorithm [24]. The convection-diffusion terms are discretised by a power-law scheme and the system is numerically modelled in FORTRAN. The solution domain consists of a two-dimensional uniformly-spaced staggered grid. The convergence criterion is to reduce the maximum mass residual of the grid control volume below 10^{-7}. Grid dependency is also tested in this study. The results are presented in terms of $Nu_{m,h}$, $Nu_{m,c}$ and $|\psi|_{max}$ for four grid sizes when the Rayleigh number is $Ra = 10^6$, the Hartmann number is $Ha = 0$ and the dimensionless vertical distance of the fin from the bottom wall is $Y_p = 0.5$. Tables 1a and 1b present the results of the grid dependence study for $L_p = 0.2$ and $L_p = 0.8$, respectively. It can be seen a grid size of 100×100 satisfies the grid independence.

The numerical code is validated against the results of other studies for natural convection in cavities with fins. For example, the results of the convection heat transfer in a square cavity with a thin fin obtained from the present model are validated against the results obtained by Shi and Khodadadi [25]. Fig. 2a presents the variation of the average Nusselt number ratio with the fin position (S_p=1-Y_p) at $Ra = 10^4$. The present code has further been validated against the results of other studies for magneto-hydrodynamic buoyancy-induced convection in cavities. For example, the results for the natural convection in an inclined cavity in a magnetic field obtained from the present model are validated against the solution developed by Pirmohammadi and Ghassemi [26]. Fig. 2b presents the variation of the maximum stream function ($|\psi|_{max}$) with the cavity angle at various values of Hartmann number ($Ra = 10^5$). The validation study confirms a good agreement between the present study and the results of other studies that have been reported in the literature.

4. ANN and ANFIS Structures and Training

For the ANN and ANFIS analysis, six input parameters and four output parameters are defined. The input parameters are the Rayleigh number (Ra), the Hartmann number (Ha), the dimensionless location and length of the thin fin (Y_p and L_p), and the dimensionless coordinates (X and Y). The output parameters are the stream function (ψ), the dimensionless temperature (θ), the average Nusselt number at the cold surface ($Nu_{m,c}$) and the average

Nusselt number at the hot surface ($Nu_{m,h}$). It must be noted that X and Y are only used in determining ψ and θ. It is well understood that the number of layers, the number of neurons in each layer and the appropriate transfer function of each neuron can significantly affect the benefits and abilities of ANNs. Figure 3 shows that the feed forward ANN structure consists of three layers: input layer, hidden layer and output layer. Three continuous and differentiable transfer functions of Hyperbolic Tangent Sigmoid, Logarithmic Sigmoid, and Pure Linear are examined for all neurons in each layer, and the Hyperbolic Tangent Sigmoid transfer function is selected that provides the highest accuracy.

Figure 4 shows that the ANFIS structure consists of five layers. It is noteworthy that there has not been any well-established method that can determine the number of layers in each network and the number of neurons in each layer. It is also impractical to directly determine the Transfer Functions of each layer in the ANN and the Membership Functions (MFs) in the ANFIS. Therefore, a trial and error process has to be carried out to determine these parameters. To accomplish this, more than five hundred networks with different structures are tested and their results (error in estimating outputs) are compared. The use of the Root Mean Square of Error (RMSE) between the pattern outputs and the predicted outputs (with same inputs) is one of the conventional criteria for evaluating the performance of the ANN and ANFIS models.

$$\mathrm{RMSE} = \sqrt{\frac{1}{N}\sum(\omega_m - \omega_p)^2} \tag{9}$$

The selection of the MFs in the ANFIS architecture affects the behaviour of the model. In this study, four different MFs with Bell-Shaped, Triangular-Shaped, Trapezoidal-Shaped and Gaussian-Shaped are tested. The Triangular-Shaped MF is finally selected for all cases as it is associated with the minimum value of RMSE.

In all cases, the input-output data set is randomly divided into two (training and evaluating) subsets. For each case, two-thirds of the data is selected as the training subset and one-third as the evaluating subset. Training of the ANN is accomplished with the first subset in 1000 epochs (training stage) with the BPE (Back Propagation of Error) procedure. The BPE algorithm uses an iterative steepest descent gradient algorithm to minimize the mean squared error by regulating the weights properly. All the ANN related simulations are carried out with Neural Network toolbox of the MATLAB. The training of the ANFIS is also accomplished using the first subset in 100 epochs with hybrid (BPE for nonlinear parameters and the least square errors for linear parameters) procedure. All the ANFIS simulations are carried out using the Fuzzy toolbox of MATLAB [27].

5. Results and Discussions

ANN and ANFIS approaches are developed to study the effects of a magnetic field on the natural convection in a square cavity with a thin fin. A CFD simulation is also carried out and the CFD results are used to provide the required information for the ANN and ANFIS training and evaluation. The effects of pertinent parameters on the fluid flow and heat transfer characteristics are studied; among these are the Rayleigh number ($10^3 \le \mathrm{Ra} \le 10^6$), the Hartmann number ($0 \le \mathrm{Ha} \le 100$), the position of the thin fin ($0.1 \le Y_p \le 0.9$) and the length of the thin fin ($0 \le L_p \le 0.8$).

5.1. ANN and ANFIS versus CFD

In this section, the results of ANN and ANFIS analyses are compared with the results of CFD modelling. At first, the results for $L_p = 0.4$ and $Y_p = 0.5$ are presented in Figures 5 and 6 and in Table 2; following this the results for different values of L_p and Y_p are presented in Table 3.

Figure 5 shows the streamlines (top) and isotherms (bottom) obtained from CFD, ANFIS and ANN analyses for $\mathrm{Ra} = 10^5$ and $\mathrm{Ha} = 50$. It is evident that there are only minor differences between the CFD results and the other two analyses, particularly with regards to the ANFIS results. The streamlines show that there are two circulating cells at the top and bottom of the cavity. These circulations are generated due to the existence of the thin fin. The isotherms are intensified in the vicinity of the bottom part of the hot wall and also near the top part of the cold wall. This is an indication of higher heat transfer rates in these regions. This is also demonstrated in Figure 6. In this figure, the results of the ANN, ANFIS and CFD analyses for the local Nusselt number on the hot and cold walls are plotted. Firstly, the results show a good agreement between the three analyses. Secondly, the results indicate higher heat transfer rates at the top of the cold wall and at the bottom of the hot wall. The local Nusselt number on the hot wall (Nu_h) is zero at the centre of the hot wall ($Y = 0.5$) where the fin with the uniform temperature of T_h is located. Nu_h increases towards the top and bottom sections of the hot wall. The rate of this increase is much higher at the bottom section of the hot wall than at the top section. The reason for this is that the bottom section of the hot wall is approached by the fluid with relatively lower temperatures flowing in the bottom section of the cavity and away from the cold wall. The local Nusselt number on the cold wall increases from the bottom to the top section of the cold wall. The reason for this is that the top section of the cold wall is approached

by the fluid with relatively higher temperatures moving in the top section of the cavity and away from the hot wall.

A comparison study between the CFD modelling and the ANFIS and ANN analyses for some cases is presented in Tables 2a and 2b, respectively. The results are presented in terms of the numerical values of the average Nusselt number on the hot and cold walls ($Nu_{m,h}$ and $Nu_{m,c}$) and the maximum stream function ($|\psi|_{max}$) for two values of the Rayleigh number ($Ra = 10^3, 10^5$) and three values of Hartmann number ($Ha = 0, 50, 100$). Table 2a shows that the maximum difference between the CFD and ANFIS results is 2.20% for $Nu_{m,h}$ and Table 2b shows that the maximum difference between the CFD and ANN results is 5.07% for $|\psi|_{max}$.

Table 3 presents a comparison between CFD, ANFIS and ANN in terms of the values of the average Nusselt number on the hot and cold walls for various values of the length and position of the fin. The results show that the maximum difference between the CFD simulation and the other two analyses is 2.16%. Table 4 presents the values of RMSE and R square indexes related to ANFIS and ANN analyses for the average Nusselt number simulation cases. The ANFIS results show a higher accuracy than the ANN results. The average CPU time consumed for the CFD analysis is much larger than that consumed for ANFIS and ANN (all simulations are developed by a Pentium five computer with a 3 GHz CPU clock frequency).

Now that the precision and accuracy of the ANFIS and ANN structures have been tested, these trained structures can be used to quickly and accurately investigate the effects of various parameters on the thermal performance of the cavity.

5.2. Effects of magnetic field

In this section, ANFIS and ANN are used to examine the effects of the magnetic field on the fluid flow and heat transfer performance of the cavity. Here, the length and position of the fin are assumed to be fixed ($L_p = 0.4$ and $Y_p = 0.5$).

Figure 7 presents the streamlines (top) and isotherms (bottom) for three values of the Hartmann number ($Ha = 0, 50, 100$). The Rayleigh number is considered to be $Ra = 10^6$. Small differences can be observed between the results of ANFIS and ANN. Both analyses show the significant effects of the Hartmann number on the flow and temperature patterns in the cavity.

In the absence of the magnetic field ($Ha = 0$), a clockwise circulation covers the entire cavity transferring heat from the hot wall to the cold wall. When the magnetic field is activated, the strength of the circulating cell decreases and additional circulating cells appear at the top and bottom sections of the cavity. These cells imply inverse effects on the heat transfer process. The results also show that as the Hartmann number increases, the intensity of isotherms in the vicinity of the vertical walls decreases, which results in lower heat transfer rates.

Figure 8 is plotted to clearly demonstrate an understanding of the effects of the magnetic field on the heat transfer performance of the cavity. The results, which are determined by ANFIS and ANN, are presented in terms of the variation of an average Nusselt number on the cold wall ($Nu_{m,c}$) with respect to the Hartmann number (Ha) at various values of the Rayleigh number (Ra). For all values of the Hartmann number, increasing the Rayleigh number results in higher heat transfer rates due to the stronger buoyancy-driven flows within the cavity. At low values of the Rayleigh number ($Ra = 10^3$), where the fluid velocities are low and the heat transfer is mainly due to conduction, the effect of the Hartmann number on the heat transfer rate is negligible. As the Rayleigh number increases due to the higher contribution of convective flows, the influence of the magnetic field on the heat transfer mechanism becomes more considerable. At $Ra = 10^6$, where the fluid velocities are considerable and the heat transfer is mainly due to convection, an increase of the Hartmann number results in a significant reduction of the heat transfer rate.

5.3. Effects of fin position

In this section, ANFIS and ANN are used to examine the influence of the fin position on the fluid flow and heat transfer performance of the cavity. Here, the length of the fin and the Hartmann number are assumed to be fixed ($L_p = 0.4$ and $Ha = 50$).

Figure 9 shows the streamlines (top) and isotherms (bottom) at $Ra = 10^5$ and for three different positions of the fin ($Y_p = 0.1, 0.5, 0.9$). Both ANFIS and ANN analyses show that the streamlines and isotherms are considerably affected by the fin being repositioned on the hot wall. When the fin is located at the top of the hot wall ($Y_p = 0.9$), a clockwise circulating cell appears in the cavity and the isotherms are intensified near the top of the cold wall and the bottom of the hot wall. When the fin moves towards the centre of the hot wall ($Y_p = 0.5$), extra circulating cells appear and the isotherms move away from the hot wall. This is an indication of

a lower heat transfer rate on the hot wall. When the fin moves towards the bottom of the hot wall ($Y_p = 0.1$), the streamlines form a complete circulating cell again and the isotherms move further away from the hot wall. This indicates that a further decrease in the heat transfer rate on the hot wall is expected.

To demonstrate a better understanding of the effects of the fin position on the heat transfer performance of the cavity, Figure 10 is presented. This figure shows the variations of average Nusselt numbers on the hot and cold walls ($Nu_{m,h}$ and $Nu_{m,c}$) with respect to the position of the fin (Y_p) for different values of the Rayleigh number (Ra). Insignificant differences are observed between the results of ANFIS and ANN analyses. Figures 10a-10d show that $Nu_{m,c}$ is generally higher than $Nu_{m,h}$ for all values of the Rayleigh number. This is due to the effects of the fin, which is located on the hot wall, on the flow and heat transfer process. It is also evident that, for all values of the Rayleigh number, the variation of fin position results in more noticeable changes in $Nu_{m,h}$ compared to $Nu_{m,c}$. This is because of the greater effects of the fin on the flow behaviour in the vicinity of the hot wall compared to the cold wall. As the Rayleigh number increases, the effect of the fin position on the heat transfer rate on the hot wall becomes more noticeable. For high Rayleigh numbers ($Ra = 10^5, 10^6$), where the heat transfer is mainly due to convection, the average Nusselt number on the hot wall sharply increases as the fin moves upwards. This is due to the behaviour of the convective flow circulation adjacent to the hot wall.

5.4. Effects of fin length

In this section, the fin position and the Hartmann number are assumed to be fixed ($Y_p = 0.5,\ Ha = 50$). Figure 11 shows the streamlines (top) and the isotherms (bottom) obtained from ANFIS and ANN analyses at $Ra = 10^5$ and for three different lengths of the fin ($L_p = 0,\ 0.4,\ 0.8$). For $L_p = 0$, the cavity experiences a large clockwise circulating convective flow that is the dominant heat transfer mechanism. As the length of the fin increases ($L_p = 0.4$), separate circulations appear in the top and bottom sections of the cavity. A further increase in the length of the fin ($L_p = 0.8$) results in individual flow separations in the top and bottom sections of the cavity with a small amount of flow still crossing the gap. The isotherms show that as the length of the fin increases, the temperature patterns move away from the hot wall and

become intensified near the cold wall. This is an indication of higher Nusselt numbers on the cold wall and lower Nusselt numbers on the hot wall.

Figure 12 clearly demonstrates the effects of the fin length on the average Nusselt number ratios on the hot and cold walls ($Nu_m / Nu_{m,L_p=0}$). The average Nusselt number with no fin ($Nu_{m,L_p=0}$) is considered to be the reference value. Various Rayleigh numbers ($Ra = 10^3, 10^4, 10^5, 10^6$) are considered here. It is evident that the results of ANFIS are in agreement with those obtained from ANN. At all values of the Rayleigh number, it can be observed that $Nu_m / Nu_{m,L_p=0}$ increases for the cold wall and it decreases for the hot wall as the length of the fin increases. This can be explained by the behaviour of isotherms near the hot and cold walls at different fin lengths (Figure 11). The most significant effect of the fin length on $Nu_m / Nu_{m,L_p=0}$ for both hot and cold walls can be found at low Rayleigh numbers. For $Ra = 10^3, 10^4$, conduction dominates the heat transfer process and a higher heat transfer rate is expected when the length of the fin is extended from the hot wall towards the cold wall. As the Rayleigh number increases, the convection starts to dominate the heat transfer process and that is why the influence of the length of the fin on the heat transfer rate is less pronounced.

6. Conclusions

The laminar natural convection in a square cavity with a thin fin is examined. The cavity is influenced by a uniform magnetic field. The side walls of the cavity are kept at different temperatures and the horizontal walls are thermally insulated. Adaptive Network-based Fuzzy Inference System (ANFIS) and Artificial Neural Network (ANN) approaches are developed, trained and validated using the results of Computational Fluid Dynamics (CFD) analysis. The effects of pertinent parameters such as the Rayleigh number ($10^3 \le Ra \le 10^6$), the Hartmann number ($0 \le Ha \le 100$), the position of the thin fin ($0.1 \le Y_p \le 0.9$) and the length of the thin fin ($0 \le L_p \le 0.8$) on the fluid flow and heat transfer characteristics are studied. The results of this study lead to the following conclusions:

The flow and temperature fields and the heat transfer rate of the cavity are all influenced by the magnetic field, especially at higher Rayleigh numbers. As the Hartmann number increases, the magnetic field limits the convective flow circulations and, as a result, the heat transfer rate decreases.

The position of the fin has more noticeable effects on the heat transfer of the hot wall than that on the cold wall at higher values of the Rayleigh number where the heat transfer is mainly due to convection. The average Nusselt number on the hot wall increases significantly as the fin moves upwards along the hot wall.

The length of the fin has a stronger effect on the heat transfer rate for both hot and cold walls at low Rayleigh numbers, where the heat transfer is mainly due to conduction. For all Rayleigh numbers, as the length of the fin increases, the heat transfer rate increases for the cold wall and decreases for the hot wall. It is evident that ANFIS and ANN can successfully predict the fluid flow and heat transfer behaviour within the cavity in less time without compromising accuracy.

References

[1] M. Moreau, Magnetohydrodynamics, Kluwer Acadamic Publishers, The Netherlands, (1990).

[2] H. Ozoe, K. Okada, The effect of the direction of the external magnetic field on the three-dimensional natural convection in a cubical enclosure, International Journal of Heat and Mass Transfer, 32 (10) (1989) 1939-1954.

[3] J.P. Garandet, T. Alboussiere, R. Moreau, Buoyancy driven convection in a rectangular enclosure with a transverse magnetic field, International Journal of Heat and Mass Transfer, 35 (4) (1992) 741-748.

[4] M. Venkatachalappa, C.K. Subbaraya, Natural convection in a rectangular enclosure in the presence of a magnetic field with uniform heat flux from the side walls, Acta Mechanica, 96 (1-4) (1993) 13-26.

[5] S. Alchaar, P. Vasseur, E. Bilgen, Natural convection heat transfer in a rectangular enclosure with a transverse magnetic field, Journal of Heat Transfer, 117 (3) (1995) 668-673.

[6] N. Rudraiah, R.M. Barron, M. Venkatachalappa, C.K. Subbaraya, Effect of a magnetic field on free convection in a rectangular enclosure, International Journal of Engineering Science, 33 (8) (1995) 1075-1084.

[7] M.C. Ece, E. Buyuk, Natural-convection flow under a magnetic field in an inclined rectangular enclosure heated and cooled on adjacent walls, Fluid Dynamics Research, 38 (8) (2006) 564-590.

[8] G.S. Dulikravich, M.J. Colaco, Convective heat transfer control using magnetic and electric fields, Journal of Enhanced Heat Transfer, 13 (2) (2006) 139-155.

[9] M.A. Teamah, Numerical simulation of double diffusive natural convection in rectangular enclosure in the presences of magnetic field and heat source, International Journal of Thermal Sciences, 47 (3) (2008) 237-248.

[10] S. Sivasankaran, A. Malleswaran, J. Lee, P. Sundar, Hydro-magnetic combined convection in a lid-driven cavity with sinusoidal boundary conditions on both sidewalls, International Journal of Heat and Mass Transfer, 54 (1-3) (2011) 512-525.

[11] K. Kahveci, S. Oztuna, MHD natural convection flow and heat transfer in a laterally heated partitioned enclosure, European Journal of Mechanics, B/Fluids, 28 (6) (2009) 744-752.

[12] M. Sathiyamoorthy, A. Chamkha, Effect of magnetic field on natural convection flow in a liquid gallium filled square cavity for linearly heated side wall(s), International Journal of Thermal Sciences, 49 (9) (2010) 1856-1865.

[13] L. Fausett, *Fundamentals of Neural Networks*. 2004: Pearson Education.

[14] S. Haykin, *Nueral Networks*. 2001, Singapore: Addison Wesley Longman Pte. Ltd.

[15] A. Kargar, B. Ghasemi, S.M. Aminossadati, An artificial neural network approach to cooling analysis of electronic components in enclosures filled with nanofluids, Journal of Electronic Packaging, 133,011010 (2011) 1-9.

[16] S.M. Aminossadati, A. Kargar, B. Ghasemi, Adaptive network-based fuzzy inference system Analysis of mixed convection in a two-sided lid-driven cavity filled with a nanofluid, International Journal of Thermal Sciences, 51(2) (2012) 102-111.

[17] M.A. Mahmoud, A.E. Ben-Nakhi, Neural networks analysis of free laminar convection heat transfer in a partitioned enclosure, Communications in Nonlinear Science and Numerical Simulation, 12 (7) (2007) 1265-1276.

[18] T.V.V. Sudhakar, C. Balaji, S.P. Venkateshan, Optimal configuration of discrete heat sources in a vertical duct under conjugate mixed convection using artificial neural networks, International Journal of Thermal Sciences, 48 (5) (2009) 881-890.

[19] A. Ozsunar, E. Arcaklloglu, F. Nusret Dur, The prediction of maximum temperature for single chips' cooling using artificial neural networks, Heat and Mass Transfer/Waerme- und Stoffuebertragung, 45 (4) (2009) 443-450.

[20] B. Kosko, *Neural Networks and Fuzzy Systems, A Dynamical System Apoproach*. 1991, NJ: Prentice Hall, Englewood Cliffs.

[21] J.S.R. Jang, ANFIS: Adaptive Network Based Fuzzy interference systems, IEEE Transactions on Systems, Man, and Cybernetics, 23 (3) (1993) 665-685.

[22] Y. Varol, E. Avci, A. Koca, H.F. Oztop, Prediction of flow fields and temperature distributions due to natural convection in a triangular enclosure using Adaptive-Network-Based Fuzzy Inference System (ANFIS) and Artificial Neural Network (ANN), International Communications in Heat and Mass Transfer, 34 (7) (2007) 887-896.

[23] Y. Varol, A. Koca, H.F. Oztop, E. Avci, Analysis of adaptive-network-based fuzzy inference system (ANFIS) to estimate buoyancy-induced flow field in partially heated triangular enclosures, Expert Systems with Applications, 35 (4) (2008) 1989-1997.

[24] S.V. Patankar, Numerical heat transfer and fluid flow, Hemisphere Publishing Corporation, Taylor and Francis Group, New York (1980) 113-137.

[25] X. Shi, J.M. Khodadadi, Laminar natural convection heat transfer in a differentially heated square cavity due to a thin fin on the hot wall, Journal of Heat Transfer, 125 (4) (2003) 624-634.

[26] M. Pirmohammadi, M. Ghassemi, Effect of magnetic field on convection heat transfer inside a tilted square enclosure, International Communications in Heat and Mass Transfer, 36 (7) (2009) 776-780.

[27] The MathWorks Inc., MATLAB Version 7.10.0.499, R2010a (2010).

Tables

Table 1a: The effects of grid on results ($Ra = 10^6$, $Ha = 0$, $L_p = 0.2$, $Y_p = 0.5$)

Grid	20×20	60×60	100×100	140×140
$Nu_{m,h}$	9.166	8.017	7.801	7.735
$Nu_{m,c}$	10.637	9.731	9.583	9.550
$\lvert\psi\rvert_{max}$	24.147	20.376	19.790	19.614

Table 1b: The effects of grid on results ($Ra = 10^6$, $Ha = 0$, $L_p = 0.8$, $Y_p = 0.5$)

Grid	20×20	60×60	100×100	140×140
$Nu_{m,h}$	7.292	6.388	6.217	6.168
$Nu_{m,c}$	11.629	10.939	10.841	10.827
$\lvert\psi\rvert_{max}$	19.647	19.182	19.166	19.211

Table 2a: A comparison between CFD and ANFIS analyses in terms of the average Nusselt numbers for the hot and cold walls and the maximum stream function ($L_p = 0.4$, $Y_p = 0.5$)

Ra	Ha	$Nu_{m,h}$			$Nu_{m,c}$			$\lvert\psi\rvert_{max}$		
		CFD	ANFIS	Difference (%)	CFD	ANFIS	Difference (%)	CFD	ANFIS	Difference (%)
10^3	0	0.455	0.455	0.00	1.278	1.278	0.00	0.481	0.481	0.00
	50	0.443	0.443	0.00	1.256	1.256	0.00	0.047	0.047	0.00
	100	0.443	0.449	1.35	1.256	1.269	1.04	0.014	0.014	0.00
10^5	0	2.968	3.023	1.85	4.871	4.871	0.00	10.505	10.538	0.31
	50	1.318	1.318	0.00	2.476	2.476	0.00	3.390	3.398	0.24
	100	0.636	0.650	2.20	1.531	1.531	0.00	1.279	1.281	0.16

Table 2b: A comparison between CFD and ANN analyses in terms of the average Nusselt numbers for the hot and cold walls and the maximum stream function ($L_p = 0.4$, $Y_p = 0.5$)

Ra	Ha	$Nu_{m,h}$			$Nu_{m,c}$			$\lvert\psi\rvert_{max}$		
		CFD	ANN	Difference (%)	CFD	ANN	Difference (%)	CFD	ANN	Difference (%)
10^3	0	0.455	0.455	0.00	1.278	1.278	0.00	0.481	0.484	0.62
	50	0.443	0.443	0.00	1.256	1.271	1.19	0.047	0.048	2.13
	100	0.443	0.443	0.00	1.256	1.256	0.00	0.014	0.014	0.00
10^5	0	2.968	2.968	0.00	4.871	4.871	0.00	10.505	10.193	2.97
	50	1.318	1.318	0.00	2.476	2.476	0.00	3.390	3.218	5.07
	100	0.636	0.636	0.00	1.531	1.531	0.00	1.279	1.223	4.38

Table 3: A comparison between the results of CFD and the results of ANFIS and ANN in terms of the average Nusselt numbers for hot and cold walls ($Ra = 10^5$, $Ha = 50$)

L_p	Y_p	$Nu_{m,h}$					$Nu_{m,c}$				
		CFD	ANFIS	Difference (%)	ANN	Difference (%)	CFD	ANFIS	Difference (%)	ANN	Difference (%)
0	0.5	2.170	2.170	0.00	2.182	0.55	2.170	2.170	0.00	2.145	1.15
0.4	0.5	1.318	1.318	0.00	1.318	0.00	2.476	2.476	0.00	2.476	0.00
0.8	0.5	0.786	0.769	2.16	0.786	0.00	3.519	3.519	0.00	3.519	0.00
0.4	0.1	0.640	0.640	0.00	0.640	0.00	2.519	2.519	0.00	2.519	0.00
0.4	0.9	1.979	1.979	0.00	1.979	0.00	2.353	2.353	0.00	2.353	0.00

Table 4: A comparison between CFD, ANFIS and ANN in terms of the values of RMSE, R square and CPU times related to the average Nusselt number for the hot and cold walls

	$Nu_{m,h}$			$Nu_{m,c}$		
	CFD	ANFIS	ANN	CFD	ANFIS	ANN
RMSE	-	0.0109	0.0286	-	0.0138	0.0495
R^2	-	0.99997	0.99979	-	0.99997	0.99965
CPU Time	320-600 (s)	35-45 (ms)	30-39 (ms)	320-600 (s)	35-45 (ms)	30-39 (ms)

Figures

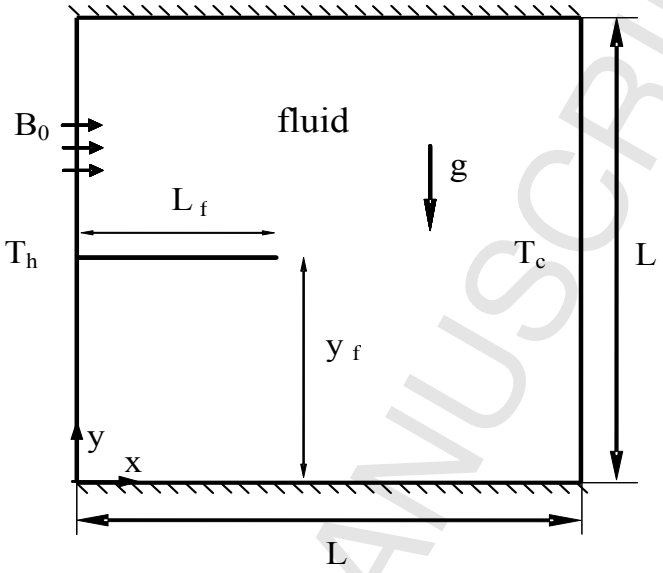

Figure 1: A schematic diagram of the physical model

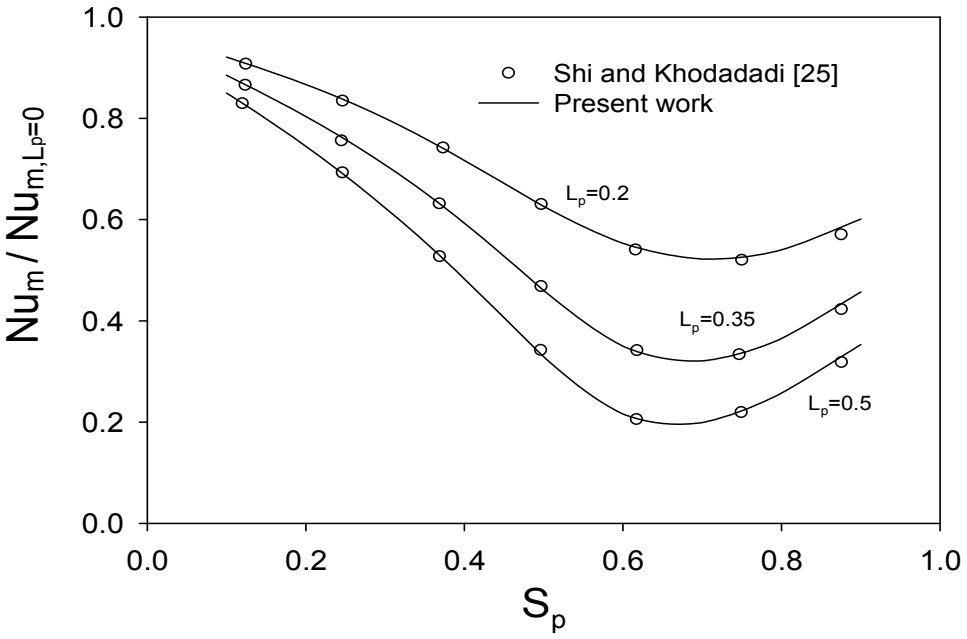

Figure 2a: Validation of the present code for natural convection heat transfer inside a cavity with a thin fin against Shi and Khodadadi [25]

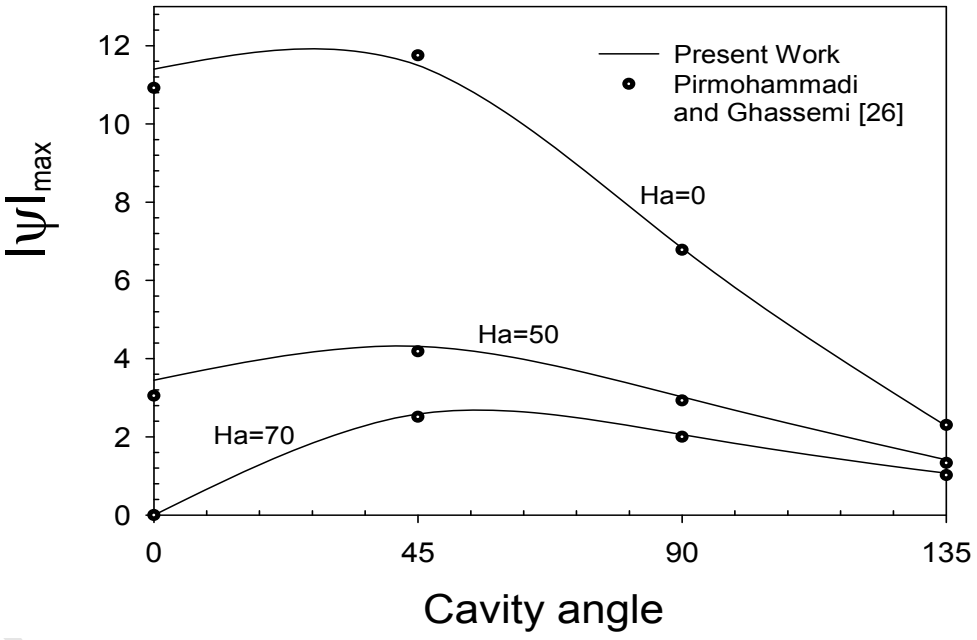

Figure 2b: Validation of the present code for convection heat transfer with magnetic field inside a cavity against Pirmohammadi and Ghassemi [26]

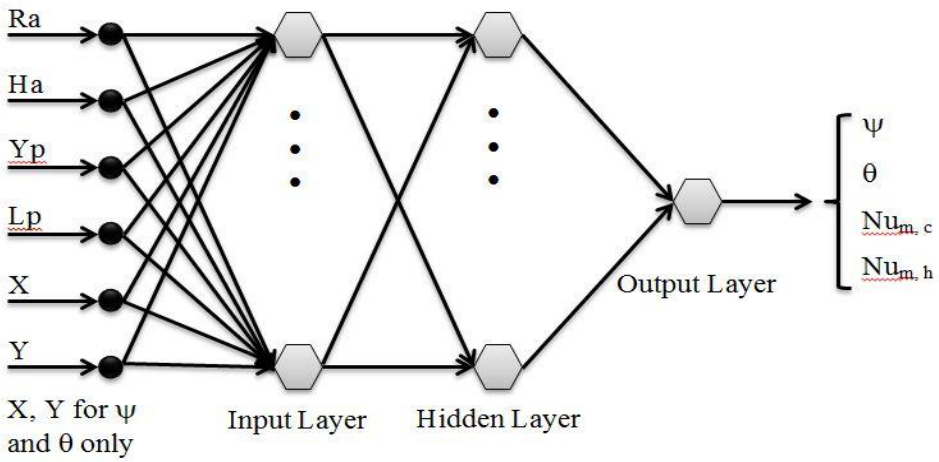

Figure 3: ANN structure

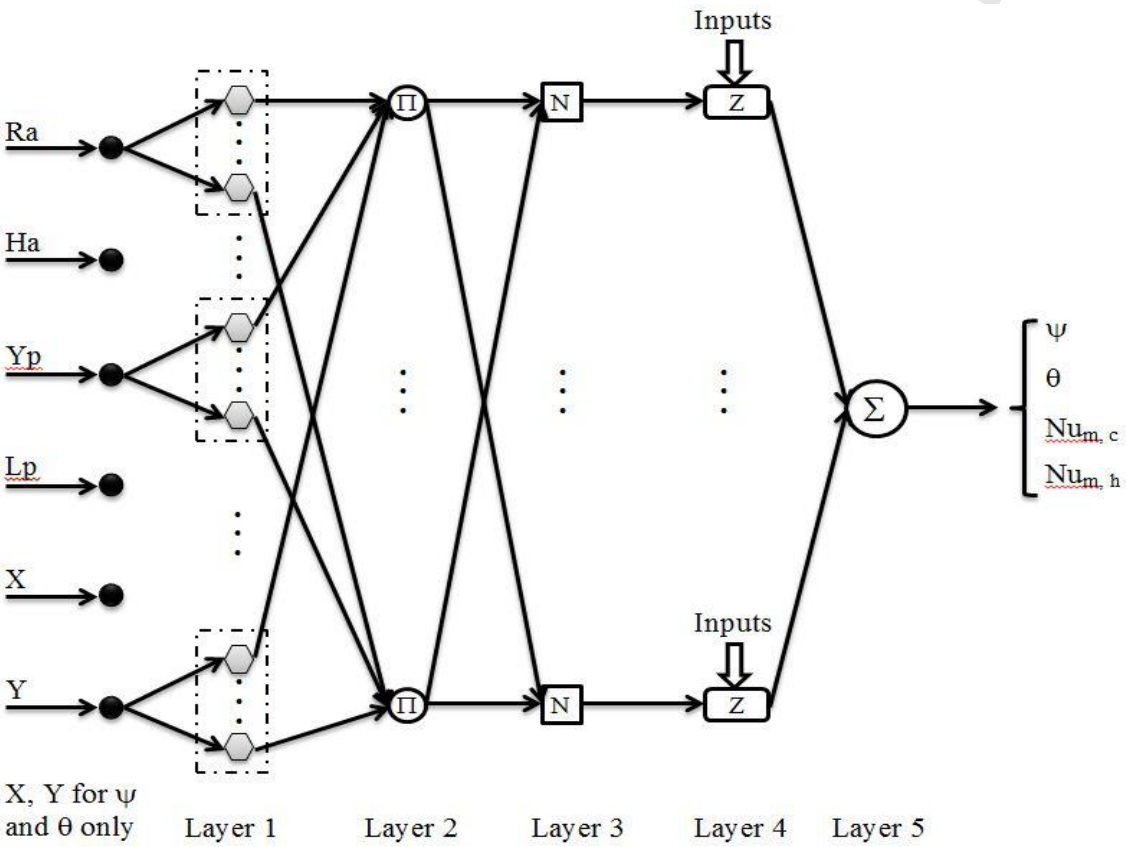

Figure 4: ANFIS structure

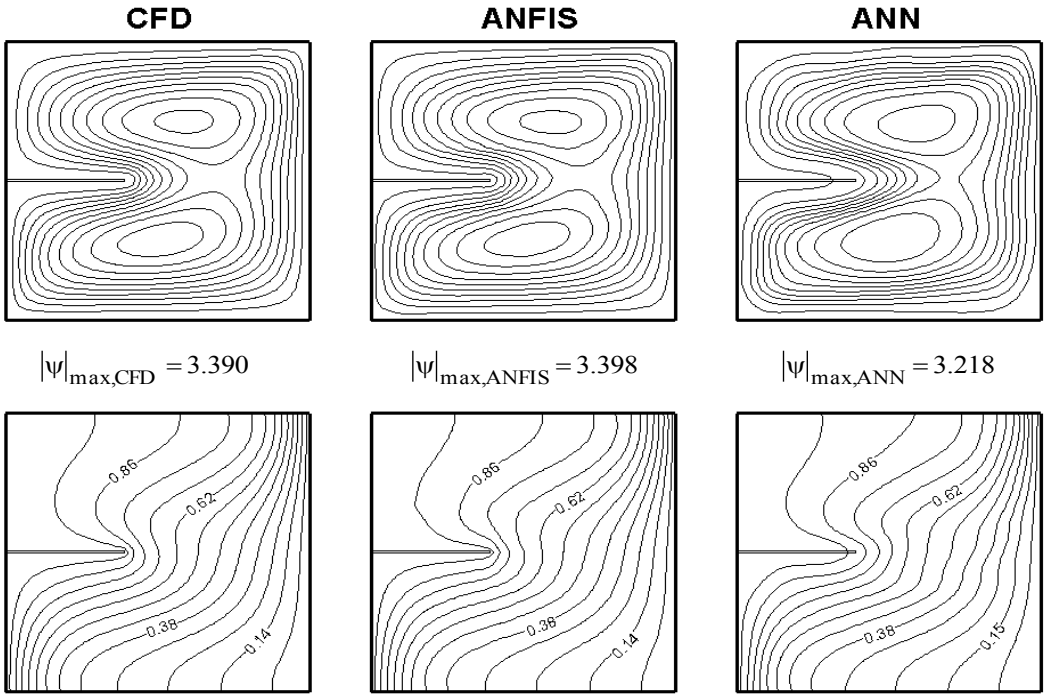

Figure 5: Streamlines (top) and isotherms (bottom) from CFD, ANFIS and ANN ($Ra = 10^5$, $Ha = 50$, $L_p = 0.4, Y_p = 0.5$)

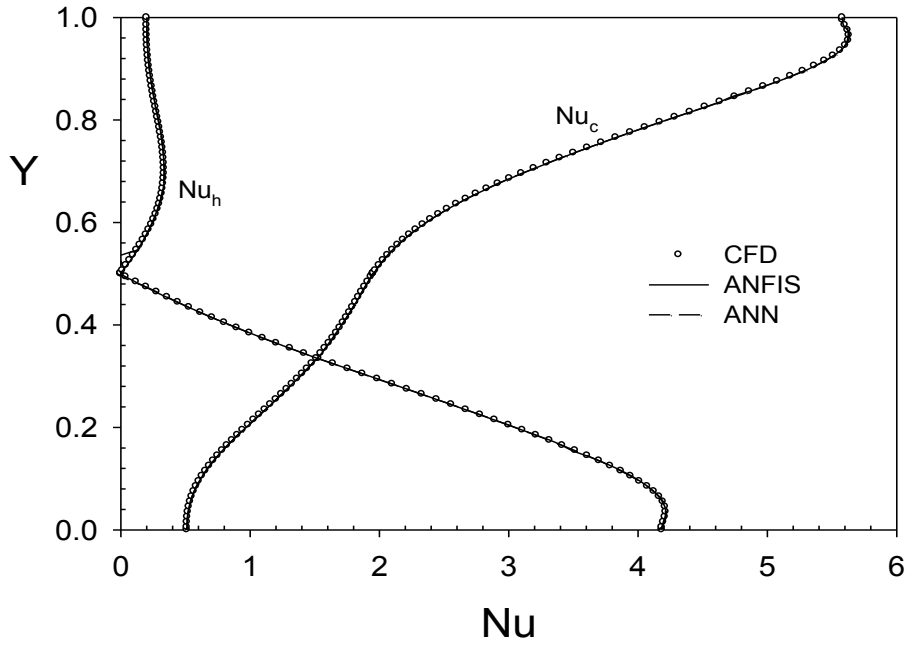

Figure 6: Variation of local Nusselt number along the hot and cold walls from CFD, ANFIS and ANN ($Ra = 10^5$, $Ha = 50$, $L_p = 0.4, Y_p = 0.5$)

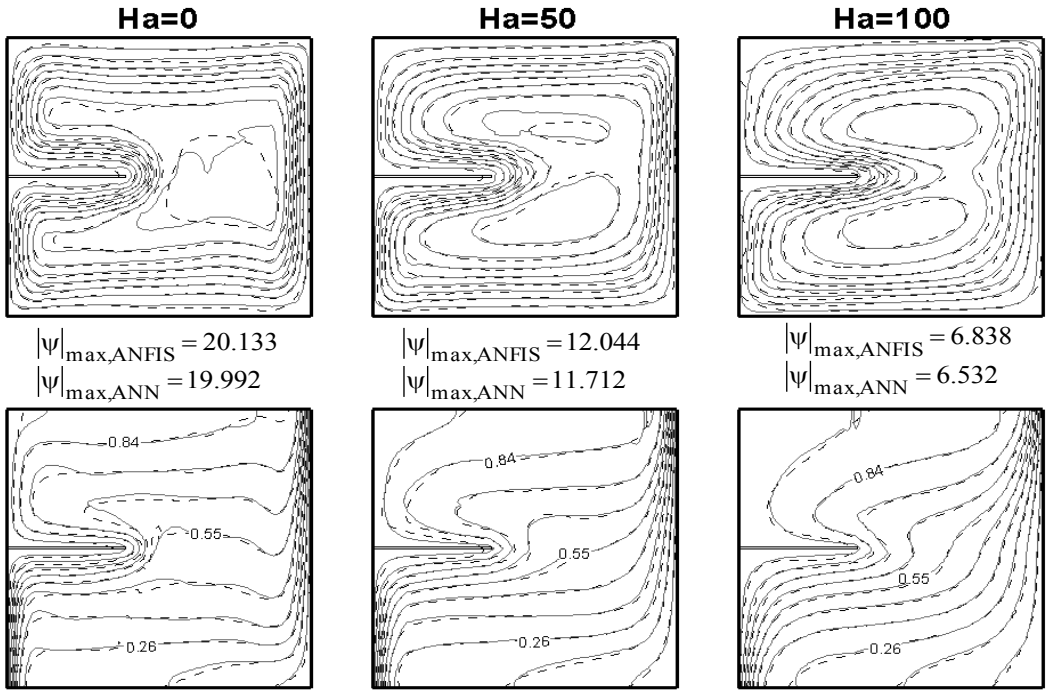

Figure 7: Streamlines (top) and isotherms (bottom) from ANFIS (—) and ANN (---) at different Hartmann numbers ($Ra = 10^6$, $L_p = 0.4$, $Y_p = 0.5$)

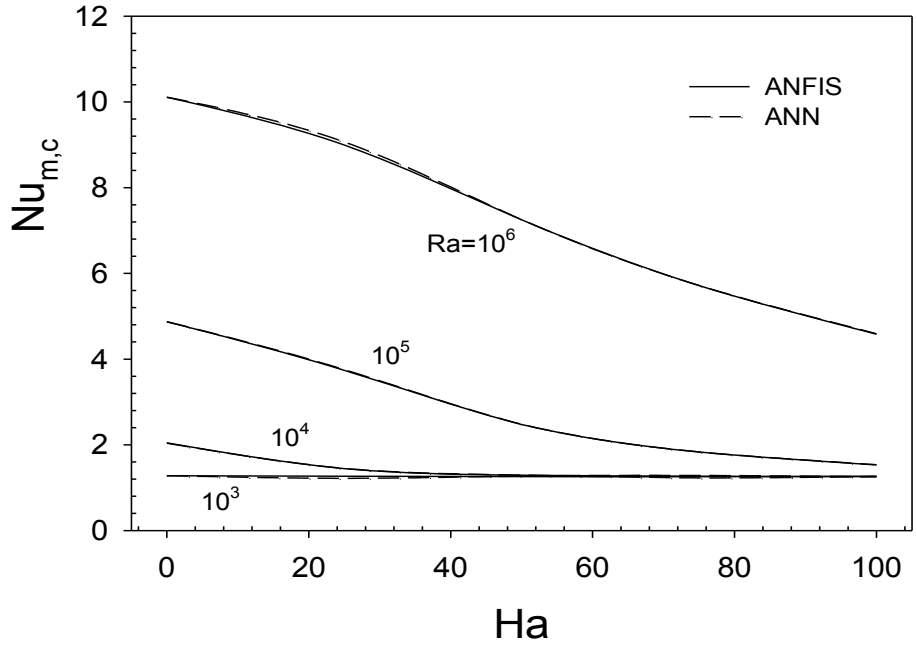

Figure 8: Variation of average Nusselt number on the cold wall with Hartmann number from ANFIS and ANN ($L_p = 0.4$, $Y_p = 0.5$)

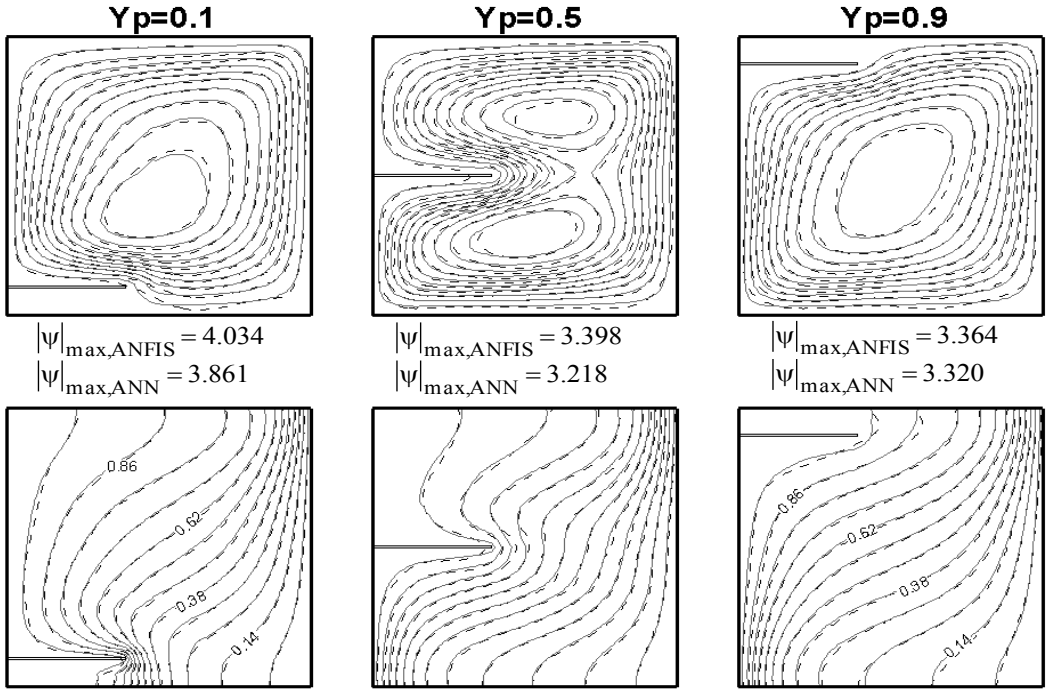

Figure 9: Streamlines (top) and isotherms (bottom) from ANFIS (—) and ANN (---) at different fin positions ($Ra = 10^5$, $Ha = 50$, $L_p = 0.4$)

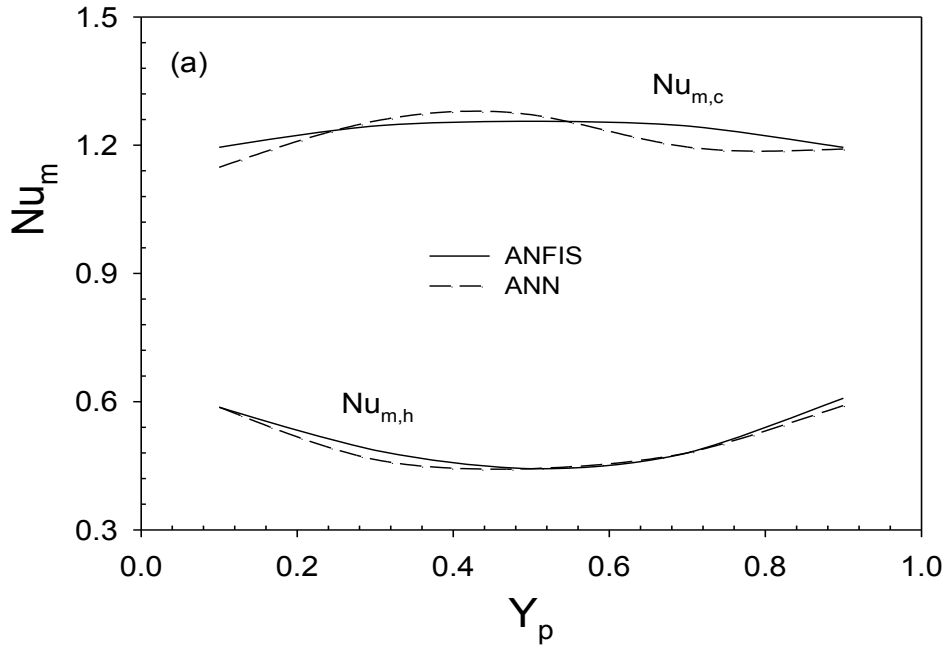

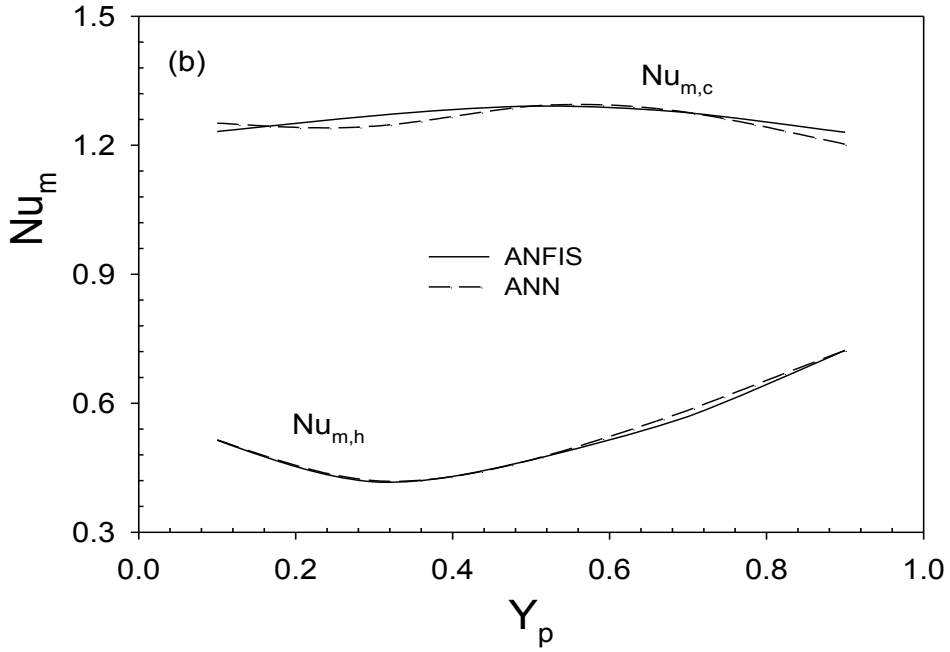

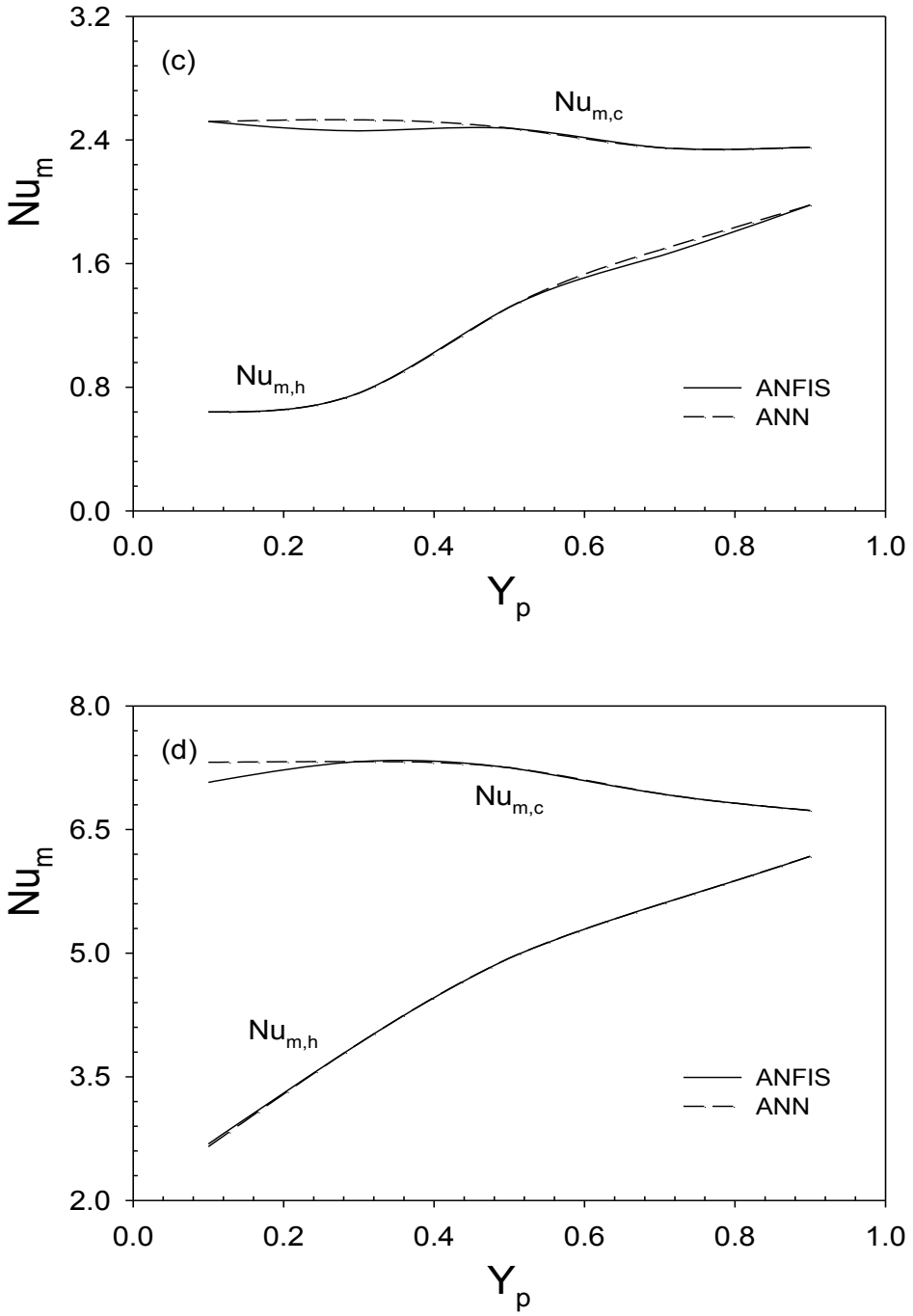

Figure 10: Variation of average Nusselt number on the hot and cold walls with the fin position from ANFIS and ANN ($Ha = 50,\ L_p = 0.4$)

(a)$Ra = 10^3$, (b) $Ra = 10^4$, (c) $Ra = 10^5$, (d) $Ra = 10^6$

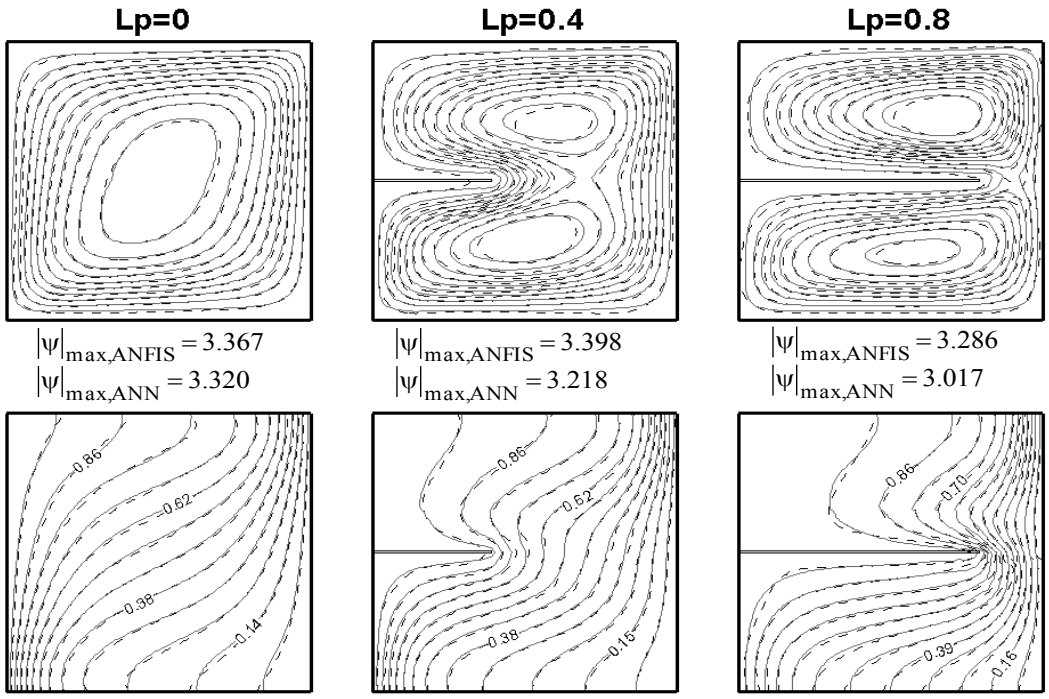

Figure 11: Streamlines (top) and isotherms (bottom) from ANFIS (—) and ANN (---) at different fin lengths ($Ra = 10^5$, $Ha = 50$, $Y_p = 0.5$)

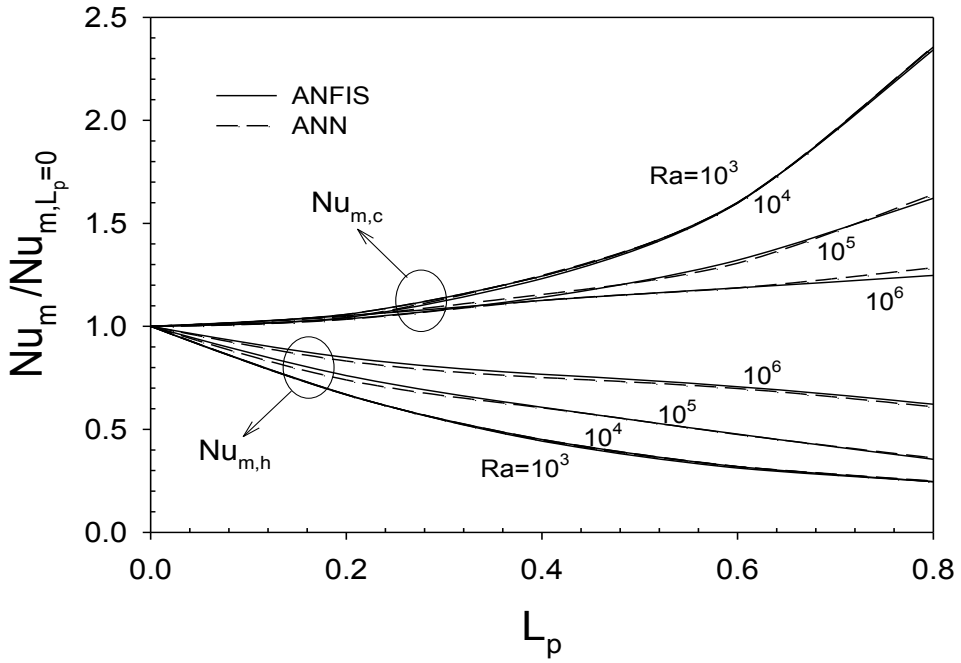

Figure 12: Variation of average Nusselt number ratio with the fin length from ANFIS and ANN ($Ha = 50,\ Y_p = 0.5$)